Electronic Supplementary Material (ESI) for Journal of Materials Chemistry A.

Nanoscale *in situ* Detection of Nucleation and Growth of Li Electrodeposition at Various Current Densities

Haesung Jung[1], Byeongdu Lee[2], Miklos Lengyel[1], Richard Axelbaum[1], Jeeyoung Yoo[3], Youn Sang Kim[3], and Young-Shin Jun[1,*]

[1]*Department of Energy, Environmental and Chemical Engineering, Washington University, St. Louis, Missouri, 63130, United States*

[2]*X-ray Science Division, Argonne National Laboratory, Argonne, Illinois 60439, United States*

[3]*Program in Nano Science and Technology, Graduate School of Convergence Science and Technology, Seoul National University, Seoul 151-742, Republic of Korea*

Electronic supplementary information

Table of Contents:

S1. Fitting methods for grazing incidence small angle X-ray scattering patterns.

The detected scattering patterns give information about particle sizes and fractal behaviors. 2D transmission GISAXS images were cut to reduce them to 1D intensity profiles. The profiles were modeled by eqn (S1):[1-3]

$$I(q) = N \cdot P(q,R,\rho) \cdot S(q, I_{pow}, \mu, R_h, \upsilon_f) \quad \text{(S1)}$$

$$P(q,R,\rho) = \Delta\rho^2 \int D(R,\sigma) V^2(R) \, |F(q,R)|^2 dR \quad \text{(S2)}$$

$$S\left(q, I_{pow}, \mu, R_h, \upsilon_f\right) = I_{pow} q^{\mu} + S(q, R_h, \upsilon_f) \quad \text{(S3)}$$

where N is the number density, $P(q, R, \sigma)$ is the particle form factor, q is the scattering vector, R is the radius, σ is the standard deviation, V is the particle volume, and $S(q, I_{pow}, \mu, R_h, v_f)$ is the structural factor. The form factor can be decomposed as eqn (S2). $\Delta\rho$ is the difference in scattering length densities between particles and background, and $D(R, \sigma)$ is the Schultz distribution for polydisperse size particles:

$$D(R,\sigma) = (z+1)^{z+1} \left(\frac{R}{R_0}\right)^z \frac{exp\left[-(z+1)\left(\frac{R}{R_0}\right)\right]}{R_0 \Gamma(z+1)} \qquad \text{for } z > -1 \quad \text{(S4)}$$

$$z = \left(\frac{R_0}{\sigma}\right)^2 - 1 \quad \text{(S5)}$$

where R_0 is the average radius, and z is the width parameter. $F(q, R)$ is the scattering amplitude of the sphere with radius R, $F(q,R) = (3\,sin(qR) - qR\,cos(qr))/(qR)^3$.[4] A spherical shape was modeled for the primary particles because the initial particles are likely too small to be faceted. The structure factor describes the spatial distribution of the individual particles. As shown in eqn (S3), the structure factor can be decomposed into two hierarchical levels of the large aggregate system composed of small primary particles.[1] $I_{pow}q^{-\mu}$ is the power law, which explains the fractal behavior of aggregated primary Li particles.[5, 6] I_{pow} is a factor weighting the intensity contribution

from the power law, μ is the exponent of power law, which is the slope of the power law at log-log scale. S(q, R_h, v_f) represents the hard-sphere Percus-Yevick model, with R_h and v_f being the hard-sphere interaction distance and volume fraction respectively. For dilute systems, the structure factor is equal to one.[2]

The fitted values of R and σ under various current densities and time lapses were used to calculate the radii of gyration (R_g) of the primary particles, according to the Schultz distribution function given by $R_g = R_0\sqrt{\frac{3(z+8)(z+7)}{5(z+1)^2}}$.[7] The fitted total particle number (N) was in arbitrary units (comparable within this study) because $\Delta\rho$ was an assumed number and intensity was not calibrated using standard samples. To the best of our knowledge, a calibration standard for GISAXS intensity has not yet been developed.[2] Under each current density condition, the distribution of primary particle sizes was determined. The aggregated particle sizes could not be analyzed because the q regime was beyond the detectable range of our transmission GISAXS experimental setting. Although we could not analyze the aggregated particle size, in a log q versus log $I(q)$ plot, the slope of the power law at small q gives fractal information about the aggregated particles. All data analyses were performed with the Igor Pro program (V. 6.22A, WaveMetrics, Inc., Oregon).

The measured intensity of transmission GISAXS comes from the electron density difference with the background. The lower electron density of the deposited Li (ρ = ~0.14 Å^{-3}) than the stainless steel substrate (ρ = ~2.20 Å^{-3}) and electrolyte (ρ = ~0.40 Å^{-3}) has a distinct electron density difference between the particles and background, which can be observed from transmission GISAXS measurements. At the initial stage of the electrodeposition process, a solid electrolyte interface (SEI) is produced from decomposition of the electrolyte.[8, 9] The initial SEI

layer suppresses further SEI growth by blocking contact between the electrolyte and active electrode surface.[10] During charging, the SEI layer is formed mostly when the voltage passes 0.5 V ~ 0.7 V (vs Li^+/Li).[11] In our transmission GISAXS measurement, there was no discernible change of intensity at the initial formation of the SEI layer by electrodeposition. The voltage exceeded the SEI formation regime (0.5 V ~ 0.7 V (vs Li^+/Li)) at ~100 seconds (0.1 mA/cm^2), ~50 seconds (0.5 mA/cm^2), and ~5 seconds (2 mA/cm^2). However, the intensity of transmission GISAXS was not changed at these time points. An increased intensity of transmission GISAXS was observed after the voltage reached a flat plateau with a negative potential (Fig. S2), which is the condition for nucleation and growth by Li electrodeposition.[12, 13] Previous studies of Li-ion batteries using SAXS measurement also showed that observing SEI formation using SAXS is unfeasible, due to the weakly scattering SEI layer.[9, 14, 15] Therefore, the intensity change from SEI layer growth in our measurement can be considered negligible.

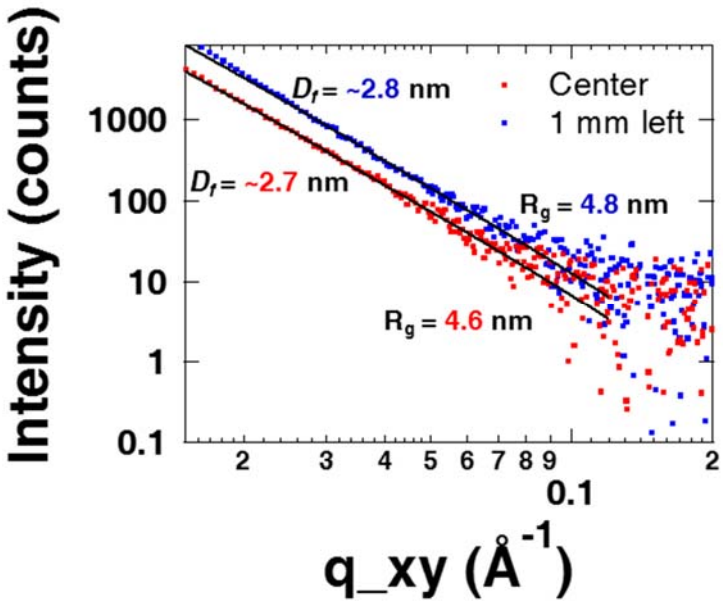

Fig. S1. Representative beam interaction tests at 0.5 mA/cm^2 after 1 hr experiment. The possibility of beam interaction was tested by comparing the center position of the cell with the cell moved 1 mm aside from the center. The center position was exposed to the X-ray beam continuously for 10 seconds and then unexposed for 10 seconds. This cycle was repeated for 1 hr. The 1 mm left position was exposed for only 10 seconds at 1hr. Because the edge of the SS substrate is rough from being cut, transmission GISAXS intensity can be variable at two different positions of the same cell. Therefore, an absolute comparison of intensity is not feasible. However, the two positions show similar particle sizes and fractal dimensions. Therefore, we can rule out the effect of beam interaction in analyzing particle size and fractal dimension during Li electrodeposition.

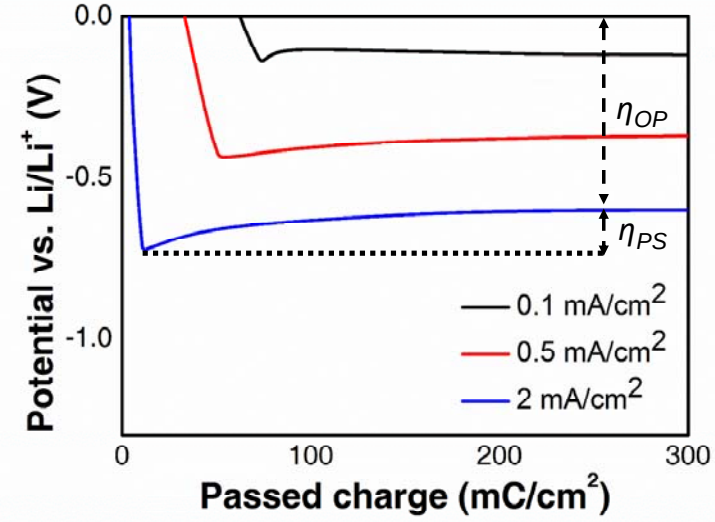

Fig. S2. Potential changes during Li electrodeposition process under various current densities. The higher current density has a larger potential spike (η_{PS}), which is obtained by subtracting the overpotential at the potential spike from the saturated overpotential η_{OP}.

The relation between critical nucleus size of Li particles and overpotential can be expressed by Nernst equation:[12]

$$E^* = E_0 + \frac{RT}{F} ln \frac{a^{Li^+}_{electrolyte}}{a_{ad}} \quad \text{(S6)}$$

where E^* is the potential during the Li electrodeposition, E_0 is the equilibrium potential, a_{ad} is the activity of adsorbed Li^+ at the polarized condition, $a^{Li^+}_{electrolyte}$ is the activity of Li^+ in the electrolyte, R is the gas constant, T is the absolute temperature, and F is Faraday's constant. Under the equilibrium state, the Nernst equation is expressed by

$$E = E_0 + \frac{RT}{F} ln \frac{a^{Li^+}_{electrolyte}}{a^0_{ad}} \quad \text{(S7)}$$

The overpotential, ΔE, is derived from the potential change, $\Delta E = E^* - E$. From the overpotential equation, the increase of a_{ad} can be formulated under a higher overpotential condition, [12]

$$a_{ad} = a_{ad}^0 exp\left(\frac{F\Delta E}{RT}\right) \quad \text{(S8)}$$

The chemical potential for the accommodation of Li^+ into a nucleation embryo can be defined as follows,

$$\Delta\varphi = F\Delta E \quad \text{(S9)}$$

Therefore, the higher overpotential increases the chemical potential during polarization. The chemical potential in systems affects the critical nucleus size:

$$r_c = \frac{2\gamma_{NE}\Omega}{\Delta\varphi} = \frac{2\gamma_{NE}\Omega}{F\Delta E} \quad \text{(S10)}$$

where r_c is the critical nuclei size, γ_{NE} is the interfacial free energy between the nucleus and electrolyte, and Ω is the molecular volume of the Li nanoparticles. From this relation, the increase of overpotential results in the decrease of critical nuclei size.[12]

Table S1. Overpotential changes observed from potential spikes under various current densities in triplicate tests.

Current density [mA cm^{-2}]	Potential spike (η_{PS}) [mV]
0.1	36 ± 9
0.5	79 ± 12
2	273 ± 35

In Fig. S2, the potential profiles during Li electrodeposition are plotted for three current densities. Previous studies reported that a potential spike, η_{PS}, which is obtained from the

subtraction of the overpotential at the potential spike from the saturated overpotential, η_{OP}, relates to the overpotential.[12] The profiles show that the higher current density condition has larger spike peaks. Although a measurement of accurate overpotential value cannot be obtained from this potential spike, the trend of η_{PS} in Table S1 is consistent with our expectation and observations from transmission GISAXS analyses.

References

1. Y. Hu, B. Lee, C. Bell and Y.-S. Jun, *Langmuir*, 2012, **28**, 7737-7746.
2. Q. Li, A. Fernandez-Martinez, B. Lee, G. A. Waychunas and Y.-S. Jun, *Environ. Sci. Technol.*, 2014.
3. Y.-S. Jun, D. E. Giammar and C. J. Werth, *Environ. Sci. Technol.*, 2012, **47**, 3-8.
4. Y.-S. Jun, B. Lee and G. A. Waychunas, *Environ. Sci. Technol.*, 2010, **44**, 8182-8189.
5. J. Teixeira, *J. Appl. Crystallogr.*, 1988, **21**, 781-785.
6. H.-C. Liao, C.-S. Tsao, Y.-T. Shao, S.-Y. Chang, Y.-C. Huang, C.-M. Chuang, T.-H. Lin, C.-Y. Chen, C.-J. Su, U. S. Jeng, Y.-F. Chen and W.-F. Su, *Energy Environ. Sci.*, 2013, **6**, 1938-1948.
7. C. W. Neil, B. Lee and Y.-S. Jun, *Environ. Sci. Technol.*, 2014, **48**, 11883-11891.
8. W. Xu, J. Wang, F. Ding, X. Chen, E. Nasybulin, Y. Zhang and J.-G. Zhang, *Energy Environ. Sci.*, 2014, **7**, 513-537.
9. R. L. Sacci, J. L. Bañuelos, G. M. Veith, K. C. Littrell, Y. Q. Cheng, C. U. Wildgruber, L. L. Jones, A. J. Ramirez-Cuesta, G. Rother and N. J. Dudney, *J. Phys. Chem. C*, 2015, **119**, 9816-9823.
10. H. J. Ploehn, P. Ramadass and R. E. White, *J. Electrochem. Soc.*, 2004, **151**, A456-A462.
11. C. K. Chan, H. Peng, G. Liu, K. McIlwrath, X. F. Zhang, R. A. Huggins and Y. Cui, *Nat. Nanotechnol.*, 2008, **3**, 31-35.
12. F. Sagane, K.-i. Ikeda, K. Okita, H. Sano, H. Sakaebe and Y. Iriyama, *J. Power Sources*, 2013, **233**, 34-42.
13. L. Grande, J. von Zamory, S. Koch, J. Kalhoff, E. Paillard and S. Passerini, *ACS Appl. Mater. Inter.*, 2015.
14. D. Stevens and J. Dahn, *J. Electrochem. Soc.*, 2000, **147**, 4428-4431.
15. D. Stevens and J. Dahn, *J. Electrochem. Soc.*, 2001, **148**, A803-A811.